Comprehensive approach to structure functions

A. Donnachie*
Department of Physics and Astronomy, University of Manchester, Manchester M13 9PL, United Kingdom

H. G. Dosch†
Institut für Theoretische Physik der Universität Heidelberg Philosophenweg 16, D-69120 Heidelberg, Germany
(Received 12 July 2001; published 12 December 2001)

We present a model based on a dipole picture with a hard and a soft Pomeron in which large dipoles couple to the soft Pomeron and small dipoles couple to the hard Pomeron. The parameters in the model are fixed by proton-proton scattering and the proton structure function $F_2(x,Q^2)$. The model is then applied successfully to the proton charm structure function $F_2^c(x,Q^2)$, the proton longitudinal structure function $F_2^L(x,Q^2)$, J/ψ photoproduction, deep virtual Compton scattering $\gamma^* p \to \gamma p$, the real photon-proton total cross section $\sigma_{\gamma p}^{\rm tot}(s)$, the real photon-photon total cross section $\sigma_{\gamma\gamma}^{\rm tot}(s)$, and the photon structure function $F_2^\gamma(x,Q^2)$. Differences between our predictions and data on charm production in real photon-photon interactions and the $\gamma^*\gamma^*$ cross section $\sigma_{\gamma\gamma}^{\rm tot}(s)$ are discussed.

DOI: 10.1103/PhysRevD.65.014019 PACS number(s): 13.60.Hb, 12.38.Lg

I. INTRODUCTION

The suggestion [1,2] that deep inelastic scattering at small x can be economically and successfully described by a two-component model comprising the soft nonperturbative Pomeron of hadronic interactions, with an intercept ~ 1.08, and a hard Pomeron, with an intercept ≈ 1.4, has met with considerable phenomenological success when applied to other reactions. Notable among these are J/ψ photoproduction and the charm structure function of the proton [3,2], and exclusive ρ and ϕ photoproduction at large t [4]. Successful although this phenomenology is, it does not explain, for example, the relative strengths of the hard and soft Pomeron in deep inelastic scattering or in J/ψ photoproduction, or why the charm structure function of the proton is completely dominated by the hard Pomeron.

To answer questions such as these requires a specific model for the diffractive process. This in turn necessitates consideration of the particle wave functions which enter the reactions, and to disentangle the dynamics of diffraction from wave-function effects it is necessary to treat several processes simultaneously. An example is provided by [5] in which high-energy exclusive photo- and electroproduction of vector mesons were studied in a two-component model of diffraction. The soft and hard Pomerons were modeled by nonperturbative and perturbative gluon exchange respectively. This approach has the advantage of providing a common kinematical structure in which it is possible to separate the effects of the vector-meson wave functions from the dynamics of the exchange. It was shown that the wave functions determine many aspects of the data, including some which might have been considered to reflect the dynamics of the exchange.

In this paper we follow the same philosophy and treat hadron-hadron, photon-hadron, and photon-photon reactions in a uniform approach, but with a different model for the two Pomerons. The model is based [6–8] on a dipole picture with two Pomerons in which small dipoles couple to the hard Pomeron and large dipoles to the soft Pomeron. The proton is considered as a quark-diquark system i.e. effectively as a dipole. This is very convenient but not essential for the approach [9]. The dipole-dipole cross section [10,9] has been obtained in a functional approach [11] to high-energy hadron-hadron scattering, the functional integrals being approximately evaluated in a specific nonperturbative model, the stochastic vacuum model [12,13]. This model yields confinement and relates high energy scattering with low energy data and with results of lattice gauge calculations. The total dipole-dipole cross section is obtained as the forward scattering amplitude of two dipoles averaged over all orientations. This is then transportable to any dipole-dipole-type reaction for which the wave functions of the participating particles are known.

In Sec. II we quote the results required for the present calculation and refer to the literature for motivation and justification. In Sec. III the model is applied in turn to the proton structure function $F_2(x,Q^2)$, the proton charm structure function $F_2^c(x,Q^2)$, the proton longitudinal structure function $F_2^L(x,Q^2)$, J/ψ photoproduction, deep virtual Compton scattering $\gamma^* p \to \gamma p$, the real photon-proton total cross section $\sigma_{\gamma p}^{\rm tot}(W^2)$, the real photon-photon total cross section $\sigma_{\gamma\gamma}^{\rm tot}(W^2)$, the photon structure function $F_2^\gamma(x,Q^2)$, charm production in real photon-photon interactions, and the virtual photon-photon cross section $\sigma_{\gamma^*\gamma^*}^{\rm tot}(W^2)$. The parameters for the dipole-dipole cross section are fine-tuned to proton-proton scattering and the criteria for defining small and large dipoles are obtained from the proton structure function. These parameters remain unchanged throughout, and all other processes are controlled by the relevant particle wave functions. Our conclusions are presented in Sec. IV.

II. THE MODEL

Our normalization of the forward scattering amplitude $T_{ab\to cd}$ for the reaction $ab \to cd$ is such that the forward

*Email address: ad@a3.ph.man.ac.uk
†Email address: h.g.dosch@thphys.uni-heidelberg.de

 ©2001 The American Physical Society

elastic cross section is given by

$$\left.\frac{d}{dt}\sigma_{ab\to cb}\right|_{t=t_{\min}}=\frac{1}{16\pi^2W^4}|T_{ab\to cb}|^2. \tag{1}$$

If the outgoing particle c is the same as the incoming particle a we obtain the total cross section from the optical theorem as

$$\sigma_{ab}^{\rm tot}=\frac{1}{W^2}{\rm Im}T_{ab\to ab}, \tag{2}$$

where W is the center-of-mass energy of particles a and b.

In the model one calculates the expectation value of two light-like Wilson loops with transverse extension $\vec{R}_1$ and $\vec{R}_2$. After averaging over all directions and integrating over the impact parameter one obtains the forward scattering amplitude of two dipoles [10,9]. The dipole-dipole cross section is obtained using the optical theorem (2). At $W=\sqrt{s}=20$ GeV it can be numerically approximated to an accuracy of better than 10% by the factorizing form

$$\sigma_{\rm dip}(R_1,R_2)=0.67\frac{1}{4\pi^2}(\langle g^2FF\rangle a^4)^2R_1(1-e^{-R_1/3.1a})\times R_2(1-e^{-R_2/3.1a}) \tag{3}$$

where $\langle g^2FF\rangle$ is the gluon condensate in a pure gauge theory and a is the correlation length of the gauge-invariant two-gluon correlator. The parameters are taken from lattice results [16] and fine-tuned to pp scattering:

$$a=0.346\ \text{fm},\quad \langle g^2FF\rangle a^4=23.77. \tag{4}$$

A quark-diquark picture is used for the proton so that the dipole formalism is applicable.

The model in which the cross section (3) has been obtained leads to the formation of a color-electric string between the quark and antiquark (or diquark) [14]. For small R_i the cross section (3) shows the R^2 behavior typical of dipole scattering as obtained in perturbative QCD [15]. For larger distances however, the R dependence of the cross section becomes weaker and finally linear. This linear increase of the cross section can be traced back to the interaction of the strings [9] formed between the quarks. The strings thus contribute essentially to high energy scattering. The ''dipole-dipole'' cross section parametrized in Eq. (3) is thus the result of a highly-nontrivial infrared behavior of the nonperturbative model.

The amplitude $T_{ab\to cb}$ is obtained by multiplying Eq. (3) with the products of the appropriate wave functions, using Eq. (2) and integrating

$$T_{ab\to cb}=iW^2\int d^2R_1d^2R_2\int_0^1dz_1dz_2\psi_c^*\times(\vec{R}_1,z_1)\psi_a(\vec{R}_1,z_1)|\psi_b(\vec{R}_2,z_2)|^2\sigma_{\rm dip}(R_1,R_2). \tag{5}$$

Here $\vec{R}$ is the distance vector from the quark to the antiquark or diquark and z is the longitudinal momentum fraction of the quark. It is assumed that the product $\psi_c^*(\vec{R}_1,z_1)\psi_a(\vec{R}_1,z_1)$ depends at most weakly on the polar angle ϕ of $\vec{R}$ and so the ϕ-dependence can be ignored.

For the photon wave functions we use the perturbative expressions:

$$\psi_\gamma^{\lambda=0,h,\bar{h}}(Q^2,\vec{R},z)=\sqrt{3\alpha}\hat{e}_f\frac{-2z(1-z)Q\,\delta_{h,-\bar{h}}}{2\pi}Q\,K_0(\epsilon R)$$

$$\psi_\gamma^{\lambda=\pm1,h,\bar{h}}(Q^2,\vec{R},z)=\sqrt{3\alpha}\hat{e}_f\frac{\pm\sqrt{2}}{2\pi}(i\,e^{\pm i\phi}[z\,\delta_{h,1/2}\delta_{\bar{h},-1/2}-(1-z)\,\delta_{h,-1/2}\delta_{\bar{h},1/2}]\epsilon K_1(\epsilon R)+m\,\delta_{h,\pm1/2}\delta_{\bar{h},\pm1/2}K_0(\epsilon R)) \tag{6}$$

with

$$\epsilon=\sqrt{z(1-z)Q^2+m_f^2}. \tag{7}$$

Here R and ϕ are the plane-polar coordinates of the transverse separation $\vec{R}$ of the quark-antiquark pair, $\hat{e}_f$ is the charge of the quark in units of the elementary charge, m_f its mass, and h and $\bar{h}$ the helicities of the quarks and the antiquarks; $\lambda=0$ indicates a longitudinal photon, $\lambda=\pm1$ a transverse photon. The functions K_i are the modified Bessel functions. These expressions can be used for photons of high virtuality. For photons of low virtuality we use the same expressions but with a Q^2-dependent mass $m_{\rm eff}(Q^2)$ instead of m_f. This procedure has been justified in [17] and the following linear parametrizations have been obtained from comparison with the phenomenological vector-current two-point function:

$$m_{\rm eff}(Q^2)=\begin{cases}m_f+m_{0q}(1-Q^2/Q_0^2) & \text{for}\quad Q^2\leqslant Q_0^2,\\ m_f & \text{for}\quad Q^2\geqslant Q_0^2,\end{cases} \tag{8}$$

with

$$m_{0q}=0.20\pm0.02\ \text{GeV},\quad m_f=0.007\ \text{GeV},\quad Q_0^2=1.05\ \text{GeV}^2 \tag{9}$$

for the up and down quark, and

$$m_{0q}=0.31\pm0.02\ \text{GeV},\quad m_f=0.15\ \text{GeV},\quad Q_0^2=1.6\ \text{GeV}^2 \tag{10}$$

for the strange quark. In this paper we use $m_{0q}=0.19$ GeV for the light quarks and 0.31 GeV for the strange quark. The mass of the charmed quark was chosen as the median value of the modified minimal subtraction scheme ($\overline{\rm MS}$) mass at $\mu=m_c$, $m_c=1.25$ GeV [18].

In the quark-diquark picture of the proton we use a Gaussian wave function

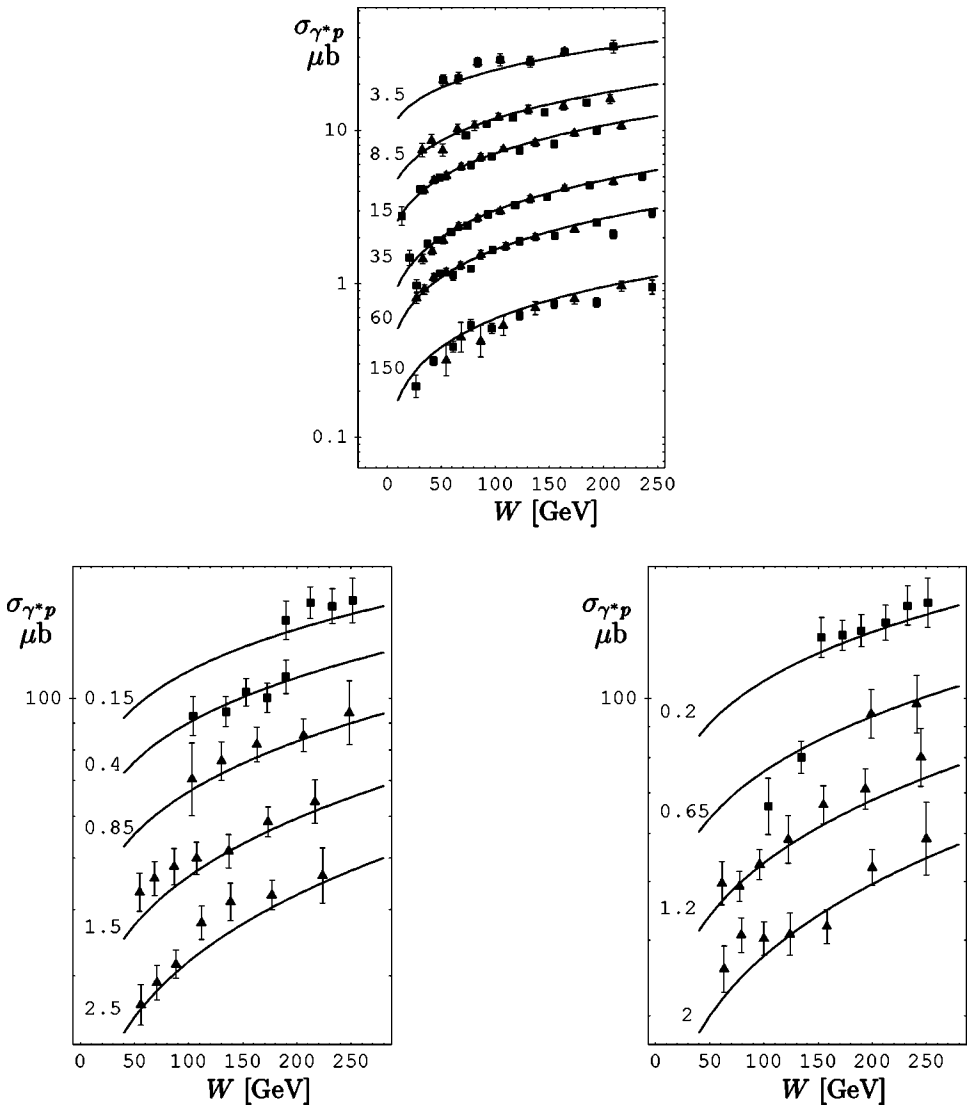

FIG. 1. Examples of $\sigma^{\rm tot}_{\gamma^* p}(Q^2,W)$ for different values of the photon virtuality Q^2 in GeV^2 as indicated in the figures. The solid line is our model. The data are from ZEUS [25], squares, and H1 [26], triangles.

$$\psi_p(\vec{R}) = \frac{1}{\sqrt{2\pi}R_p}\exp\left(-\frac{R^2}{4R_p^2}\right). \tag{11}$$

The transverse radius R_p was also fine tuned [19], in this case to obtain the observed logarithmic slope for elastic pp scattering at a center-of-mass energy of $W=20$ GeV:

$$R_p = 0.75 \text{ fm}. \tag{12}$$

The wave function for the J/ψ is taken from [19]. It is constructed in the following way. The spin structure is that of a massive vector current with mass m_c, that is it has the same structure as the charm part of the photon wave function (6). An additional z-dependent factor as introduced in [20] is also included and the dependence on the transverse distance R is modeled by a Gaussian such as (11). The mean radius is fixed by the normalization condition and the electromagnetic decay width.

The stochastic vacuum model is a model for the infrared behavior of QCD and and was applied originally to hadron-hadron scattering alone [9,21,22]. It turned out that it yielded reasonable results for photon-induced processes for photon virtualities Q^2 up to about 10 GeV^2 [19,17,23]. For higher values of Q^2 the model overestimates the cross sections. This may have the following reason. For consistency of the model with low-energy theorems the strong coupling in the infrared domain must have the frozen value [14] $\alpha_s \approx 0.57$. It is plausible that upon introduction of a hard scale through a highly-virtual photon the coupling of the gluons to the corresponding dipole is governed by that hard scale. Therefore we have rescaled the results obtained for the dipole cross section (1) by the factor

$$\frac{\alpha_s(Q^2)}{\alpha_s(0)} = \frac{1}{0.57}\,\frac{4\pi}{11\log(Q^2/Q_0^2+7.42)} \tag{13}$$

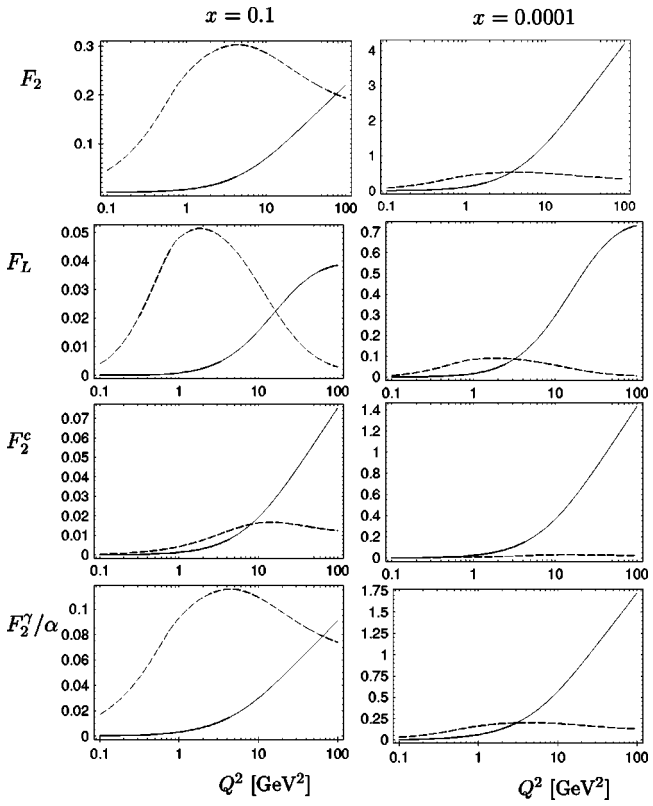

FIG. 2. The soft and hard contribution to structure functions at different values of x. Solid line hard contribution from the model; dashed line soft contribution from the model. First row, proton structure function F_2; second row, longitudinal proton structure function F_L; third row, charm contribution to the proton structure function F_2^c: last row, photon structure function F_2^γ/α.

with $Q_0^2=1$ GeV^2. This corresponds to a running coupling $\alpha_s(Q^2)$ in a flavorless scheme adjusted to give $\alpha_s(0)=0.57$.

As mentioned in the Introduction our main purpose is to apply the two-Pomeron approach to different processes. The results of [1,2] strongly suggest that the soft Pomeron couples predominantly to large dipoles whereas the hard Pomeron couples to small dipoles. In order to be economical with parameters we introduce a sharp cut and assume that only the soft Pomeron couples if both dipoles are larger than a certain value R_c, whereas the hard Pomeron couples if at least one of the dipoles is smaller than R_c. Energy dependence is introduced by hand into the dipole cross section (3) by dividing the amplitude into a soft and a hard part with the coefficients σ_s and σ_h:

$$T_{ab\to cb}(W)=iW^2(\sigma_s\ (W/W_0)^{2\epsilon_s}+\sigma_h\ (W/W_0)^{2\epsilon_h}) \tag{14}$$

with

$$W_0=20\ \text{GeV},\quad \epsilon_s=0.08,\quad \epsilon_h=0.42. \tag{15}$$

The soft Pomeron contribution is given by

$$\sigma_s=\int_{R_c}^{\infty}2\pi R_1dR_1\int_{R_c}^{\infty}2\pi R_2dR_2\int_0^1 dz_1dz_2\psi_c^*(\vec{R}_1,z_1)\times\psi_a(\vec{R}_1,z_1)|\psi_b(\vec{R}_2,z_2)|^2\sigma_{\rm dip}(R_1,R_2). \tag{16}$$

For the hard Pomeron it has been argued [24] that the appropriate dimensionless variable is RW for the following reason. Highly virtual photons have a hadronic radius $R\propto 1/Q$, so in order to ensure scaling behavior for the dimensionless quantity $Q^2\sigma_{\rm dip}(R,W)$ the W dependence should come in the combination W^2R^2 which corresponds to the inverse of the Bjorken variable x. If one dipole is small, say $R_1\leqslant R_c$, the hard contribution should depend upon the factor (R_1W); if both dipoles are small, then upon the factor $(R_1R_2W^2)$. Since the factor $W^{2\epsilon_h}$ has been extracted in Eq. (14), we obtain, for the coefficient σ_h,

$$\begin{aligned}\sigma_h=&\int_0^{R_c}2\pi R_1dR_1\int_0^{R_c}2\pi R_2dR_2\int_0^1 dz_1dz_2\psi_c^*(\vec{R}_1,z_1)\psi_a(\vec{R}_1,z_1)|\psi_b(\vec{R}_2,z_2)|^2\sigma_{\rm dip}(R_1,R_2)(R_1R_2/R_c^2)^{\epsilon_h}\\&+\int_0^{R_c}2\pi R_1dR_1\int_{R_c}^{\infty}2\pi R_2dR_2\int_0^1 dz_1dz_2\psi_c^*(\vec{R}_1,z_1)\psi_a(\vec{R}_1,z_1)|\psi_b(\vec{R}_2,z_2)|^2\sigma_{\rm dip}(R_1,R_2)(R_1/R_c)^{2\epsilon_h}\\&+\int_0^{R_c}2\pi R_2dR_2\int_{R_c}^{\infty}2\pi R_1dR_1\int_0^1 dz_1dz_2\psi_c^*(\vec{R}_1,z_1)\psi_a(\vec{R}_1,z_1)|\psi_b(\vec{R}_2,z_2)|^2\sigma_{\rm dip}(R_1,R_2)(R_2/R_c)^{2\epsilon_h}.\end{aligned} \tag{17}$$

III. RESULTS

A. γ^*p reactions

With the rescaling factor (13) and the energy dependence introduced in Eq. (17) we can describe the proton structure function, or equivalently the total γ^*p cross section $\sigma^{\rm tot}_{\gamma^*p}$, from $Q^2=0$ up to $Q^2\approx 150$ GeV^2. The only free parameter is R_c. In Fig. 1 we show some of the results for $R_c=0.22$ fm compared with a sample of experimental data from ZEUS [25] and H1 [26]. We can also compare with the fit to the data in [1] where the structure function was separated into a soft and a hard part; the model reproduces the Q^2

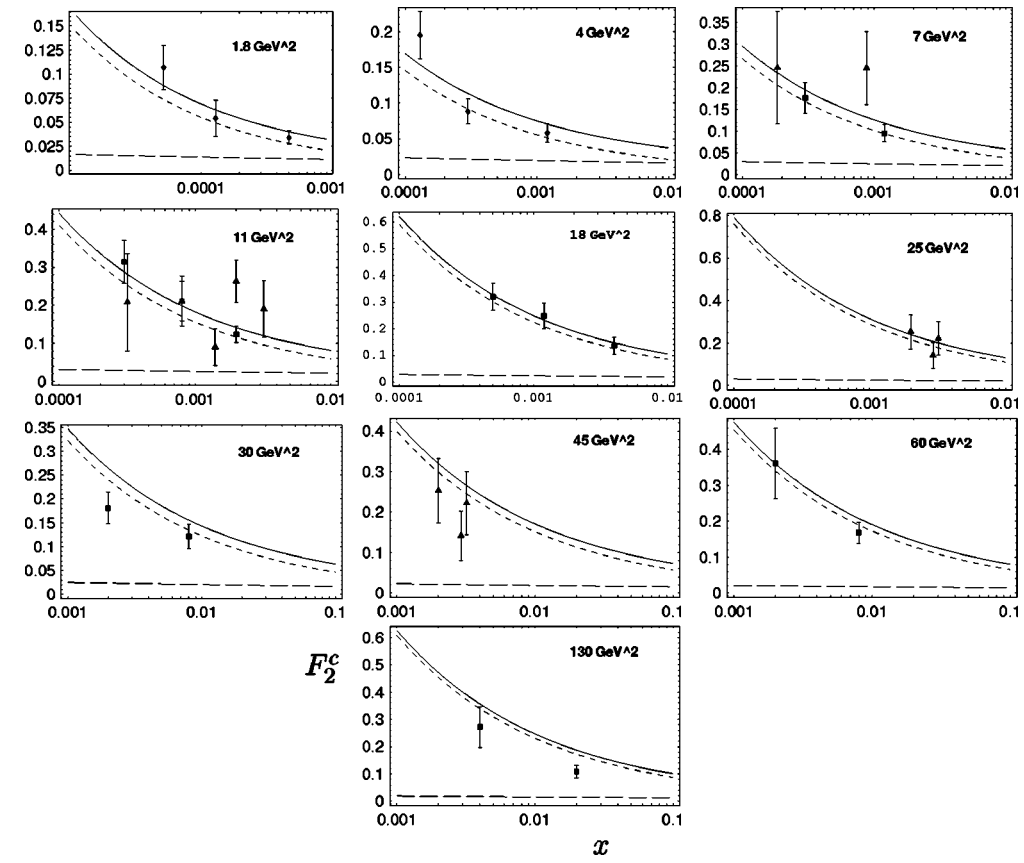

FIG. 3. The charm contribution to the proton structure function F_2^c for different values of Q^2 as indicated in the figures. The solid line is the full result, the short-dashed line the hard Pomeron contribution and the long-dashed line the soft Pomeron contribution. The data are from ZEUS [27], squares, and H1 [28], triangles.

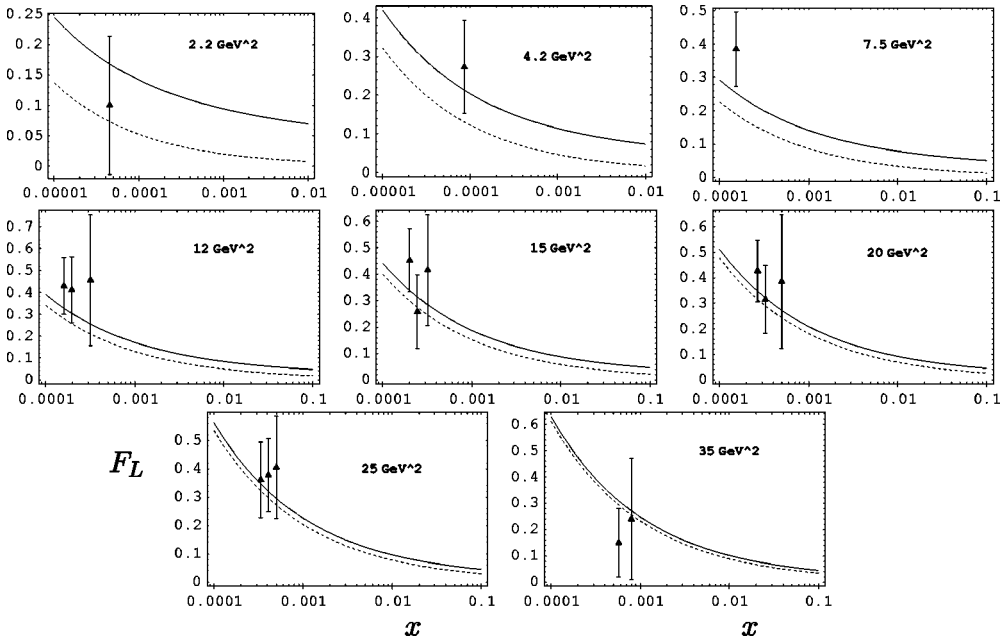

FIG. 4. The longitudinal proton structure function F_L for different values of Q^2 as indicated in the figures. The solid line is the full result and the dashed line the hard Pomeron contribution. The data are from H1 [29].

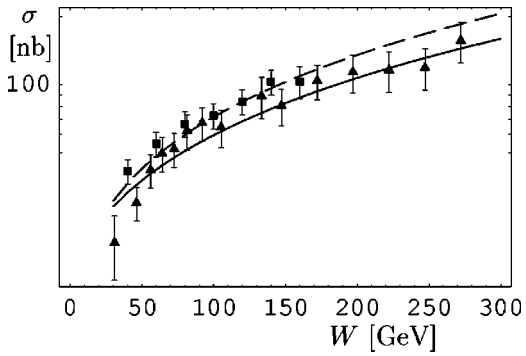

FIG. 5. Cross section for the reaction $\gamma p \to J/\psi p$. The long-dashed curve is obtained from the forward amplitude using a constant logarithmic slope $b=6$ GeV^2 and the solid curve using an s-dependent slope from Regge theory. The data are from H1 [30], triangles, and ZEUS [31], squares.

dependence of the soft- and hard-Pomeron contributions obtained in [1] very well.

With R_c fixed, the model can be used to predict the charm part of the proton structure function, $F_2^c(x,Q^2)$, and the longitudinal structure function, $F_L(x,Q^2)$. In both cases the photon wave function is concentrated at smaller distances. In the case of charm this is a consequence of the mass of the charm quark occurring in the argument ϵ [see Eq. (7)] of the modified Bessel function in the photon wave functions (6). For the longitudinal structure function it is a consequence of the factor $z(1-z)$ in the wave function of the longitudinal photon. This factor suppresses contributions from small values of ϵ, which correspond to large distances. Thus the hard Pomeron is already dominant at moderate energies, as can be seen from the second and third rows of Fig. 2. The strong suppression of the soft Pomeron relative to the hard Pomeron in $F_2^c(x,Q^2)$, which is purely a wave-function effect, is notable and provides an explanation for the almost-complete flavor-blindness of the hard Pomeron commented on in [3,2]. Comparison of the first and second rows of Fig. 2 shows that for the longitudinal structure function the increase of the short range (hard part) with increasing Q^2 is not as strong as for the transverse structure function, a consequence of the less-singular behavior of the Bessel functions at the origin in the relevant photon wave function (K_0 *vs* K_1). Nonetheless as the long range (soft part) of the longitudinal structure function is even more suppressed at large Q^2 relative to its contribution to the transverse structure function, the hard Pomeron is dominant sooner in $F_L(x,Q^2)$ than in $F_2(x,Q^2)$. In Figs. 3 and 4 we compare the predictions of the model directly with the experimental results for the charm [27,28] and longitudinal [29] structure functions. The agreement with both data sets is clearly satisfactory.

It is instructive to compare the photoproduction of J/ψ mesons with the charm structure function F_2^c. Experiment tells us that the ratio of the soft Pomeron to the hard Pomeron is much larger for J/ψ production than for the charm contribution to the proton structure function at comparable energies. This can be easily understood in the dipole-model approach. The virtual $c\bar{c}$ pair in the photon wave function has an extension of $\approx 1/m_c$, but the J/ψ has a much larger radius, in the range from a typical hadronic radius to the Bohr radius of order $1/(\alpha_s m_c)$. Therefore the overlap of the charm part of the photon wave function with the J/ψ wave function obtains a larger contribution from distances $R > R_c$ than does the square of the charm part of the photon wave function.

In the approach presented here we can only evaluate the forward production amplitude. In an earlier investigation [19] with the same model at a center-of-mass energy of $W=20$ GeV an effective logarithmic slope of the production cross section of about 6 GeV^{-2} was found. For our calculation we have used the same J/ψ wave function as there. In Fig. 5 we show the integrated production cross section for two cases: with a constant logarithmic slope of $b=6$ GeV^{-2} (dashed line) and with a slope varying with energy as predicted from Regge theory, where the trajectory of the soft Pomeron has the slope $\alpha'_{P_s}=0.25$ GeV^{-2} and that of the hard Pomeron [3] is $\alpha'_{P_h}=0.1$ GeV^{-2} (solid line) with $b=6$ GeV^{-2} at $W=20$ GeV. The agreement with the H1 [30] and ZEUS [31] data is satisfactory in both cases. The actual normalization of the cross section is rather sensitive to the special choice of the wave function, but the energy dependence is much less so, as can be inferred from the general arguments given above.

In a recent paper [32] we investigated deep virtual Compton scattering, $\gamma^* p \to \gamma p$, in essentially the same model as here. In that paper, as in previous investigations [7,8] on $\gamma\gamma$ reactions, we used a somewhat different procedure [6] to incorporate a hard scale into the nonperturbative model. In-

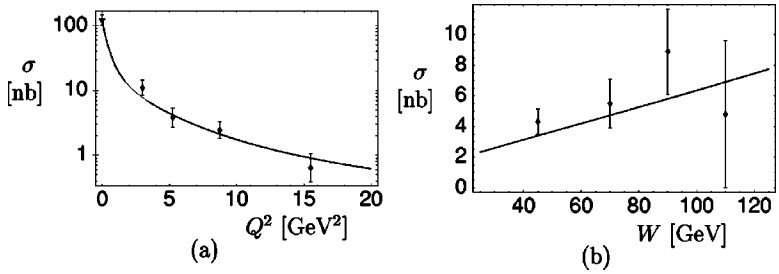

FIG. 6. (a) The integrated cross section for the reaction $\gamma^* p \to \gamma p$ as a function of the virtuality Q^2 of the incoming photon at an averaged $\langle W \rangle = 75$ GeV. (b) The integrated cross section for the reaction $\gamma^* p \to \gamma p$ as function of the center-of-mass energy W at an averaged virtuality of the incoming photon of $\langle Q^2 \rangle = 4.5$ GeV^2. The solid line is the result of the model. The data are H1 results [33].

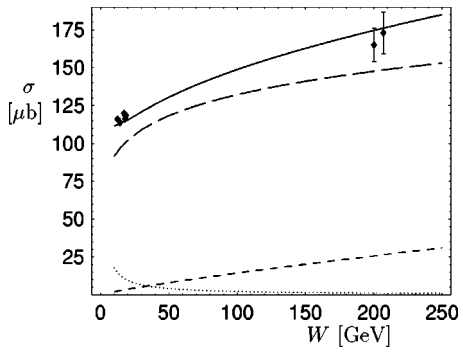

FIG. 7. $\sigma^{\rm tot}_{\gamma p}$. The solid line is the full result. It has the following contributions: long dashes, soft Pomeron; short dashes, hard Pomeron; dots, Reggeon. The data are from [34].

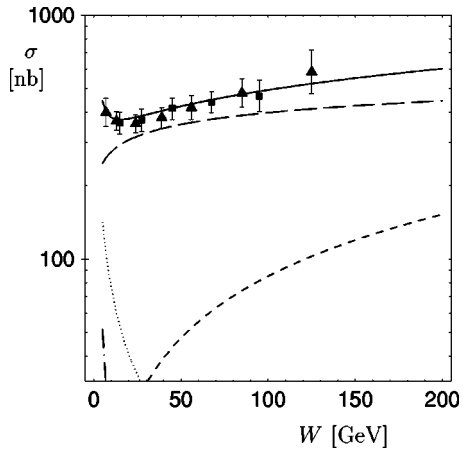

FIG. 9. $\sigma^{\rm tot}_{\gamma\gamma}(W)$. The solid line is the full result. The separate contributions are: long dashes, soft Pomeron; short dashes, hard Pomeron; dot-dashes, fixed pole (box diagram); dots, Reggeon. The data are from OPAL [36], boxes, and L3 [37], triangles.

stead of the rescaling (13) used here, in [32] the dipole cross section (3) was put to zero if at least one dipole was smaller than 0.16 fm. In Fig. 6 we show the integrated cross sections as a function of Q^2 and of W. The data are the H1 data [33] after subtraction of the Bethe-Heitler contribution. Also in this case only the forward scattering amplitude has been calculated. For comparison with experiment the integrated cross section has been obtained assuming a constant logarithmic slope $b=7$ GeV^{-2} which is the average value over the Q^2 range of the data.

We reported in [32] a serious discrepancy between the model and the preliminary data at $Q^2=3.5$ GeV^2 which was also reflected in the normalization of the integrated cross section. With the final data this discrepancy has disappeared. The difference between the results of [32] and the present calculation is smaller than the experimental error bars.

The model prediction is compared with the real γp cross section $\sigma^{\rm tot}_{\gamma p}$ in Fig. 7. Note that the model predicts a significant contribution from the hard Pomeron to $\sigma^{\rm tot}_{\gamma p}$, similar to that found in [1]. However the data do not demand such a contribution as, due to the comparatively large errors at high energy, the data can accomodate the standard soft-Pomeron energy dependence.

B. γ-γ reactions

With the same approach and the same parameters we can also calculate $\gamma\gamma$, $\gamma^*\gamma$ and $\gamma^*\gamma^*$ cross sections. Since some of the experimental results are obtained at relatively low center-of-mass energies the Reggeon contribution, Fig. 8(b), and the box diagram, Fig. 8(c), have to be taken into account. As an estimate for the Reggeon contribution we use the form given in [8]. It was pointed out there that there is considerable uncertainty in this contribution. We include this uncertainty when comparing our predictions with data. Analytical results for the box diagram without any approximations can be found in [35]. In the framework of Regge theory it correponds to a fixed pole in the angular momentum plane and has therefore to be added to the moving Regge-pole contribution [8]. In the literature it is often quoted as quark-parton-model (QPM) contribution.

The principal difference between $\gamma\gamma$ and γp at high energies comes from the singularity of the photon wave function at the origin. This favors the hard component and therefore it should become apparent even in the scattering of real photons. In Fig. 9 we show our result for the cross section $\sigma^{\rm tot}_{\gamma\gamma}$ together with OPAL [36] and L3 [37] data. The experimental cross sections are rather sensitive to the Monte Carlo model used for the unfolding of detector effects, different Monte Carlo simulations producing different results. The resulting uncertainty is contained in the errors on the OPAL data. The L3 data shown are the average of the two extremes. In this case the energy dependence of the data is not compatible with the soft Pomeron alone, and the additional contribution of the hard Pomeron is required.

The model predictions for F_2^γ/α are equally satisfactory. A comparison with data is made in Fig. 10. The agreement with experiment is good for small values of x. At large x the increasing importance of the Regge term induces an increasing uncertainty in the predictions, but nonetheless they remain satisfactory for $x\leqslant 0.1$. The model predictions for the shape of the photon structure function F_2^γ/α are very similar to those for the proton structure function, as can be seen by

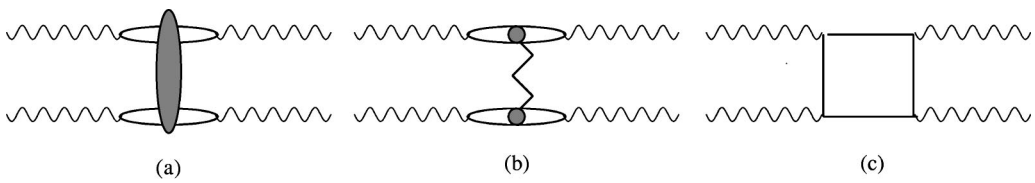

FIG. 8. Graphical representation of the dipole-dipole model contribution (a), the Reggeon contribution (b) and the box diagram (fixed pole, quark parton model) (c).

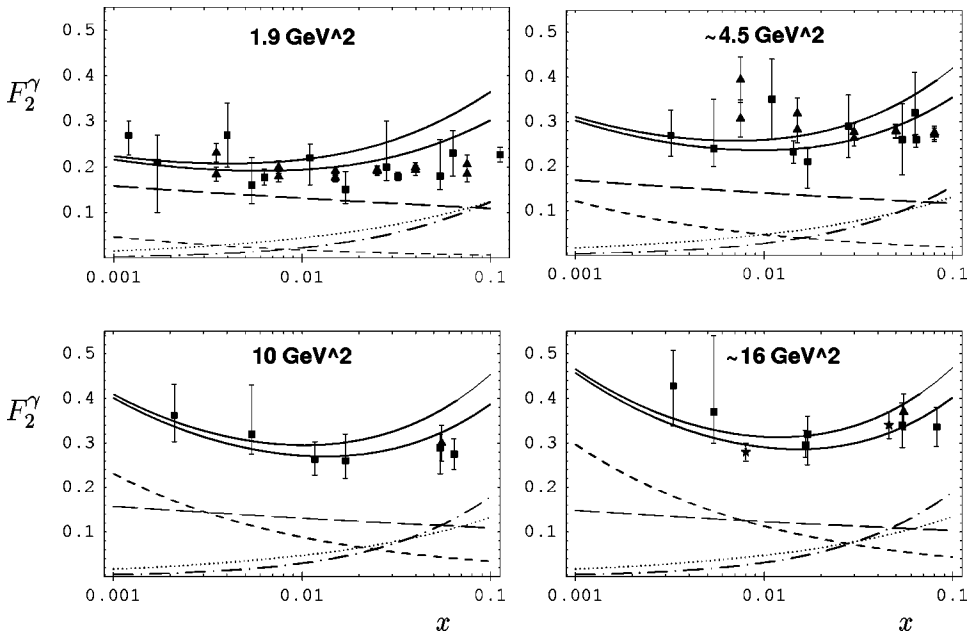

FIG. 10. The photon structure function F_2^γ/α for different values of Q^2 as indicated in the figures. The upper solid line includes the ''full Regge,'' the lower solid line includes ''half Regge.'' The separate contributions are: long dashes, soft Pomeron; short dashes, hard Pomeron; dot-dashes, fixed pole (box diagram); dots, Reggeon. The data are from OPAL [38–40], boxes; L3 [41,42], triangles; and ALEPH [43], stars.

comparing the first and last rows of Fig. 2. Indeed at large Q^2 the photon structure function exhibits precisely the same sensitivity to the hard contribution as does the proton structure function. To quantify this, in Fig. 11 we display the ratio $R=(F_2^\gamma/\alpha)/F_2$ for the soft and the hard contributions separately as a function of Q^2. The ratio of the soft contributions (dashed line) is practically constant. The hard contribution to F_2^γ is relatively favored at small Q^2, a consequence of the singularity of the photon wave function at the origin, but the ratio of the hard contributions tends to the same constant as that of the soft contributions at large Q^2. Of course this is a model-dependent statement, but nonetheless it emphasises the importance of $\sigma_{\gamma\gamma}^{\rm tot}$ as a probe of the hard contribution.

There is an interesting discrepancy between the model and the experimental results for charm production in $\gamma\gamma$ interactions. Whereas we found good agreement with experiment for the charm structure function of the proton, see Fig. 3, our model predictions for the reaction $\gamma\gamma\to c\bar{c}X$ are about a factor of 2 lower than the L3 results [44], as can be seen from Fig. 12. There is a similar discrepancy with the OPAL [45] result for the charm contribution to the photon structure function at small x, see Fig. 13, but not at larger x where the box diagram dominates. The small-x datum, taken at face value, implies that the charm contribution is already at, or close to, its asymptotic fraction of the photon structure function. Indeed, within the erors, it exhausts the full structure function.

The discrepancy cannot be removed by simple adjustments of the parameters in the model, which are anyway rather tightly constrained by other data. This can be seen from the following model-independent considerations. At very high Q^2 charm production in $\gamma^*\gamma$ scattering should be $\frac{4}{5}$ of the total cross section. A factor of $\frac{2}{5}$ comes from the ratio of the square of the charm charge to the sum of the squares of the charges of all contributing flavors, and there is an additional factor of 2 since the $c\bar{c}$ pair can be created by

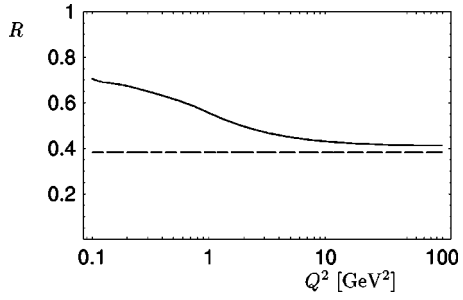

FIG. 11. R, the ratio of the soft and hard contributions of the photon to the proton structure function. The solid line is the ratio of the hard contributions; the dashed line the ratio of the soft.

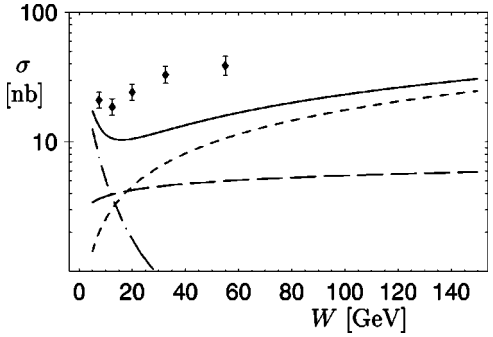

FIG. 12. Cross section for the reaction $\gamma\,\gamma\to c\bar{c}X$. The solid line is the full result. The separate contributions are: long dashes, soft Pomeron; short dashes, hard Pomeron; dot-dashes, fixed pole (box diagram). The data are from L3 [44].

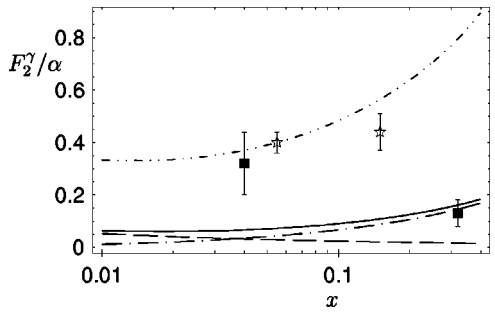

FIG. 13. Charm contribution to the photon structure function $F_{2\,c}^{\gamma}/\alpha$. The solid line is our prediction at $Q^2=20$ GeV^2, the dashed line the hard Pomeron contribution and the dotted line the contribution from the box diagram. The squares are the OPAL data [45] for charm at $\langle Q^2\rangle=20$ GeV^2. The stars are the L3 results for the full photon structure function F_2^γ at $\langle Q^2\rangle=23$ GeV^2, and the upper curve our model result for the full photon structure function F_2^γ/α at 23 GeV^2.

either photon. For moderate Q^2 one has to take account of the charm mass and make the replacement $Q^2\to Q^2_{\rm eff}$. The latter is the average of the expression $Q^2+m_c^2/(z(1-z))$ occurring in the overlap integrals. The cross section $\frac{4}{5}\sigma^{\rm tot}_{\gamma^*\gamma}(Q^2_{eff})$ is then an estimate for charm production in $\gamma\gamma$ interactions. A similar argument can be applied to γp reactions, where $\frac{2}{5}\sigma^{\rm tot}_{\gamma^* p}(Q^2_{eff})$ is the corresponding estimate for charm production with a photon of virtuality Q^2. As the product $z(1-z)\leqslant\frac{1}{4}$ then $Q^2+4m_c^2$ is the lower bound of Q^2_{eff} and therefore the cross sections with that virtuality provide an upper estimate for charm production. In Fig. 14(a) we show the model prediction for the cross section for charm production off protons at $Q^2=1.8$ GeV^2 and compare it with the upper estimate $\frac{2}{5}\sigma^{\rm tot}_{\gamma^* p}(Q^2+4m_c^2)$ and the experimental data from ZEUS [27]. The comparison of the model with the estimate is reasonable and we note that the estimate indeed tends to be above the data. In Fig. 14(b), where the target is a photon instead of a proton, the experimental data from L3 [44] are larger than the upper estimate $\frac{4}{5}\sigma^{\rm tot}_{\gamma^*\gamma}(Q^2=4m_c^2)$ which in turn is larger than the model, showing approximately the same relative magnitude as in the proton case.

So the charm data may indicate that $\gamma\gamma$ and $\gamma^*\gamma$ processes are really rather different from the corresponding γp reactions. If treated in isolation, the $\gamma\gamma$ and $\gamma^*\gamma$ data can be described by:

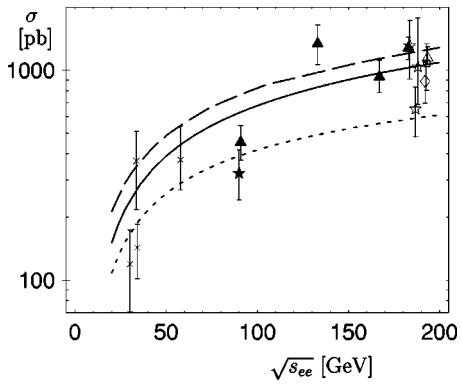

FIG. 15. Cross section for the reaction $e^+e^-\to e^+e^-c\bar{c}$. The solid line is our model with $m_c=1.25$, the dotted line the box diagram alone and the long dashed line is NLO perturbative QCD [46] with $m_c=1.3$ GeV. The data are: L3 [44], triangles; ALEPH [48], stars; DELPHI [49], diamonds; OPAL [45], boxes. The results at lower energies (crosses) are from [50–53]. Open symbols refer to preliminary results.

Increasing the fraction of the hard-Pomeron and decreasing the fraction of the soft Pomeron in $\sigma^{\rm tot}_{\gamma\gamma}$ and, possibly, giving the hard Pomeron a stronger energy dependence than we have used in our model.

Making corresponding changes in F_2^γ and modifying the Q^2 dependence of both terms, that is discarding the simple picture of Eq. (11). These modifications cannot be excluded by the present data.

Note that our calculation does not include central production of charmed quark-antiquark pairs (doubly resolved photons), but for this contribution to have a significant effect it would need to play a more important role in γ-γ collisions than in γ-proton interactions.

We note that results from perturbative QCD [46] using the photon structure function from [47] report no such discrepancy with the data. This is interesting as for γ^*p reactions the results of perturbative QCD are essentially indistinguishable from our model. The comparison between perturbative QCD and the $\gamma\gamma$ charm data was done for the full process $e^+e^-\to e^+e^-c\bar{c}$, so we have converted our $\gamma\gamma$ cross section to the full e^+e^- cross section using the equivalent photon approximation [35]. The threshold was taken as $z_{th}=4m_c^2$ and $Q^2_{max}=4m_c^2$, in the notation of [18]. The result for $m_c=1.25$ is shown in Fig. 15(a) and compared with results from perturbative QCD and experimental data. Here the

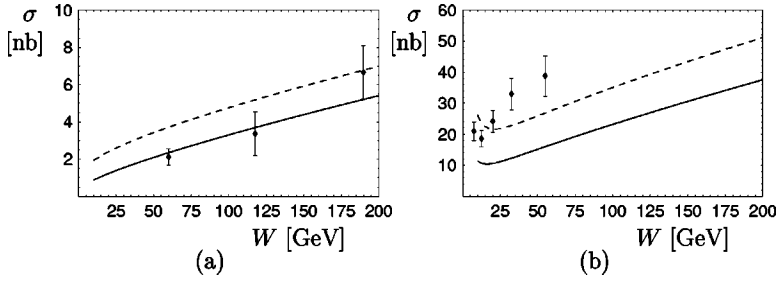

FIG. 14. Model prediction and upper estimates for the production of charm in (a) γ^*p and (b) $\gamma\gamma$ reactions. Solid line the actual model prediction; dashed line the upper estimate from flavor charge independence. The data are from [27] (a), and L3 [44] (b).

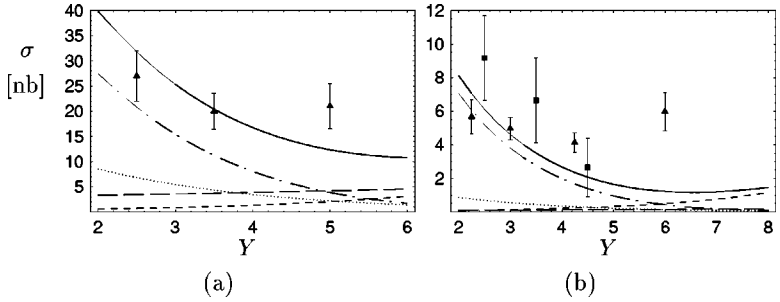

FIG. 16. $\sigma_{\gamma^*\gamma^*}$ (a) L3 data [55] at $\langle Q^2\rangle = 3.5$ GeV^2. (b) Preliminary L3 data [56] at $\langle Q^2\rangle = 15$ GeV^2, triangles and preliminary OPAL data [57] at $\langle Q^2\rangle = 16$ GeV^2, boxes. The theoretical contributions are: long dashes, soft Pomeron; short dashes, hard Pomeron; dot-dashes, fixed pole (box diagram); dots, Reggeon; solid, sum.

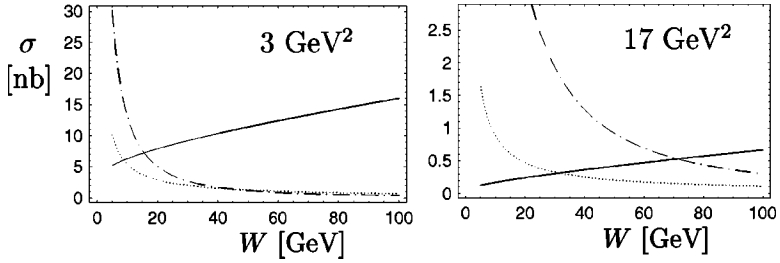

FIG. 17. Separate contributions to the $\sigma_{\gamma^*\gamma^*}(W)$ at fixed values of $Q_1^2 = Q_2^2 = Q^2$ as indicated in the figures: solid, Pomerons; dot-dashes, fixed pole (box diagram); dots, Reggeon.

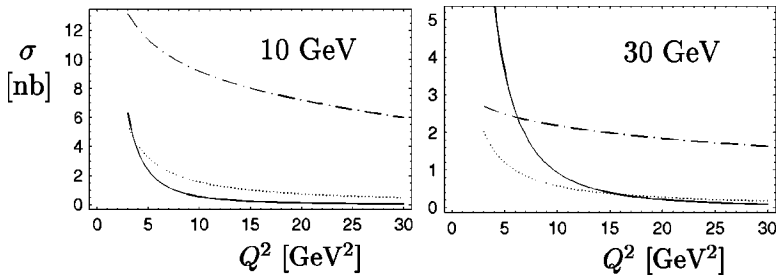

FIG. 18. Separate contributions to the $\sigma_{\gamma^*\gamma^*}(Q^2)$ at fixed values of W as indicated in the figures: solid, Pomerons; dot-dashes, fixed pole (box diagram); dots, Reggeon.

agreement with the perturbative QCD results is rather good and the discrepancy with experiment seems not dramatic. One reason for this is that the box diagram remains important up to the highest values of $\sqrt{s_{e^+e^-}}$, see Fig. 15(b), and the discrepancy at high W in Fig. 12 is smeared out in the full e^+e^- data and is much less visible. This emphasizes the importance of comparing models with $\sigma_{\gamma^*\gamma^*}$ rather than with $\sigma_{e^+e^-}$. We also note that there are significant differences at present among the preliminary data sets available, so it is perhaps too early to attempt to draw significant conclusions.

Although it is perhaps premature to draw firm conclusions from the charm data, it is clear that our nonperturbative model cannot give the full answer when both photons have high virtuality since it decreases much faster with increasing virtuality than purely perturbative contributions. The dipole-dipole cross section (3) behaves for small values of $R_1=R_2=R$ as R^4, and therefore the $\gamma^*\,\gamma^*$ cross section decreases like $1/Q^4$ for $Q^2=Q_1^2=Q_2^2$ and fixed Q^2/W^2. The perturbative contributions decrease, up to logarithms, like $1/Q^2$ [54]. This follows from a simple dimensional argument. In perturbation theory with massless quarks, in forward scattering the only dimensioned quantities are W^2 and Q^2 as no internal scale appears. Therefore for fixed Q^2/W^2 the cross section has to be proportional to $1/Q^2$ (see Fig. 16).

However our model can be used as an estimate for the nonperturbative background in $\gamma^*\gamma^*$ reactions. In Figs. 17 and 18 we show the different contributions to $\sigma^{\rm tot}_{\gamma^*\gamma^*}(Q^2)$ as a function of the common virtuality Q^2 at fixed W and as a function of W at fixed Q^2. In Fig. 16 the theoretical contributions are displayed as a function of $Y\approx\log(W^2/Q^2)$ for fixed $\langle Q^2\rangle=3.5$ and 16 GeV^2. They are compared with the L3 [55,56] and OPAL [57] data at $\langle Q^2\rangle=3.5$ and $\langle Q^2\rangle=15$ and 16 GeV^2. We note that there is evidence for a purely-nonperturbative signal visible beyond the box diagram.

C. Summary and conclusions

We have used a simple dipole-dipole approach, adopted to the two Pomeron picture [1] in order to describe a great variety of high energy reactions. The picture of dipole-dipole scattering is a consequence of our nonperturbative approach which starts from the evaluation of lightlike Wilson loops [11,10]. The dependence of the scattering amplitude on the dipole sizes is also determined in our model and related to low-energy and lattice results [12,13,9]. The energy dependence is put into the model by hand and inspired by the Q^2 dependence of the hard and soft contribution found in [1]: if at least one dipole is smaller than a critical value R_c the energy dependence is governed by the hard Pomeron, otherwise by the soft one. The numerical value $R_c\approx 0.22$ fm was adjusted from comparison with the proton structure function. With this single parameter the Q^2 dependence of the soft and hard contribution of the proton structure function obtained in [1] is reproduced very well. The behavior of different reactions is then controlled solely by the different wave function of the participating photons and hadrons. We have introduced no saturation mechanism into the dipole cross section and the analysis shows that there is no compelling reason to do so.

TABLE I. The ratio of the hard Pomeron to the total Pomeron contribution for the total cross sections of different reactions; without any unitarity corrections.

W [GeV]	pp	γp	$\gamma\gamma$
20	0.0023	0.037	0.071
100	0.007	0.10	0.19
200	0.011	0.16	0.27
1800	0.048	0.45	0.62

There is one reaction which seems to jeopardize our simple picture, namely charm production in photon-photon reactions where our model underestimates the results from L3 [44] for the reaction $\gamma\gamma\to c\bar{c}X$ by about a factor of two. We have discussed this question in detail also in an less model-dependent approach and argued that, interesting as the discrepancy is, it might be to premature to draw final conclusions. At any rate future data for this reaction might be very important for our general understanding of the underlying mechanisms of the dipole approach.

A consequence of our approach is that the hard Pomeron is not a product of perturbative evolution but is also present in soft processes. For example, we have seen that the $\gamma\gamma$ cross section receives a non-negligible hard contribution due to the pointlike coupling of the photon and the resulting singularity of the photon wave function at the origin. Similarly there is a hard contribution to the γp cross section. It is compatible with but not demanded by experiment. There is necessarily also a nonzero hard contribution to proton proton scattering. In Table I we give the ratio of the hard to the soft plus hard contribution for different reactions and center-of-mass energies. As can be seen the hard component in proton-proton scattering is so small as to be within the limits of experimental error at present energies. At higher energies, where its presence might be expected to be observable, it will be suppressed by unitarity corrections, therefore the values for proton-proton scattering represent an upper limit. As the proton, unlike the photon, is a genuinely nonperturbative object, the difficulty of detecting a hard contribution in proton proton scattering means that the γp total cross section is of considerable importance in this respect.

ACKNOWLEDGMENTS

We acknowledge helpful discussion with O. Nachtmann, H. Pirner, A. Shoshi, and F. Steffen. The work was supported in part by PPARC grant PPA/G/0/1998 and by BMBF grant 05HT1VHA/0.

[1] A. Donnachie and P.V. Landshoff, Phys. Lett. B **437**, 408 (1998).
[2] A. Donnachie and P.V. Landshoff, hep-ph/0105088.
[3] A. Donnachie and P.V. Landshoff, Phys. Lett. B **470**, 243 (1999).
[4] A. Donnachie and P.V. Landshoff, Phys. Lett. B **478**, 146 (2000).
[5] A. Donnachie, J. Gravelis, and G. Shaw, Phys. Rev. D **63**, 114013 (2001).
[6] M. Rueter, Eur. Phys. J. C **7**, 233 (1999).
[7] A. Donnachie, H.G. Dosch, and M. Rueter, Phys. Rev. D **59**, 074011 (1999).
[8] A. Donnachie, H.G. Dosch, and M. Rueter, Eur. Phys. J. C **13**, 141 (2000).
[9] H.G. Dosch, E. Ferreira, and A. Kraemer, Phys. Rev. D **50**, 1992 (1994).
[10] A. Kraemer and H.G. Dosch, Phys. Lett. B **272**, 114 (1991).
[11] O. Nachtmann, Ann. Phys. (N.Y.) **209**, 436 (1991).
[12] H.G. Dosch, Phys. Lett. B **190**, 177 (1987).
[13] H.G. Dosch and Yu.A. Simonov, Phys. Lett. B **205**, 339 (1988).
[14] M. Rueter and H.G. Dosch, Z. Phys. C **66**, 245 (1995); H.G. Dosch, O. Nachtmann, and M. Rueter, hep-ph/9503386.
[15] J.C. Collins, Phys. Rev. D **56**, 2982 (1997).
[16] M. D'Elia, A. Di Giacomo, and E. Meggiolaro, Phys. Lett. B **408**, 315 (1997).
[17] H.G. Dosch, T. Gousset, and H.J. Pirner, Phys. Rev. D **57**, 1666 (1998).
[18] Particle Data Group, D.E. Groom *et al.*, Eur. Phys. J. C **15**, 1 (2000).
[19] H.G. Dosch, T. Gousset, G. Kulzinger, and H.J. Pirner, Phys. Rev. D **55**, 2602 (1997).
[20] M. Wirbel, B. Stech, and M. Bauer, Z. Phys. C **29**, 637 (1985).
[21] E. Ferreira and F. Pereira, Phys. Lett. B **399**, 177 (1997); Phys. Rev. D **56**, 179 (1997).
[22] E. Berger and O. Nachtmann, Eur. Phys. J. C **7**, 459 (1999).
[23] G. Kulzinger, H.G. Dosch, and H.J. Pirner, Eur. Phys. J. C **7**, 73 (1999).
[24] J.R. Forshaw, G. Kerley, and G. Shaw, Phys. Rev. D **60**, 074012 (1999).
[25] ZEUS Collaboration, M. Derrick *et al.*, Z. Phys. C **72**, 3 (1996); ZEUS Collaboration, J. Breitweg *et al.*, Phys. Lett. B **407**, 432 (1997).
[26] H1 Collaboration, S. Aid *et al.*, Nucl. Phys. **B470**, 3 (1996); H1 Collaboration, C. Adloff *et al.*, *ibid.* **B497**, 3 (1997).
[27] ZEUS Collaboration, J. Breitweg *et al.*, Eur. Phys. J. C **12**, 35 (2000).
[28] H1 Collaboration, C. Adloff *et al.*, Z. Phys. C **72**, 593 (1996).
[29] H1 Collaboration, C. Adloff *et al.*, Eur. Phys. J. C **21**, 33 (2001).
[30] H1 Collaboration, C. Adloff *et al.*, Phys. Lett. B **487**, 53 (2000).
[31] ZEUS Collaboration, J. Breitweg *et al.*, Z. Phys. C **75**, 215 (1997).
[32] A. Donnachie and H.G. Dosch, Phys. Lett. B **502**, 74 (2001).
[33] H1 Collaboration, C. Adloff *et al.*, Phys. Lett. B **517**, 97 (2001).
[34] H1 Collaboration, S. Aid *et al.*, Z. Phys. C **69**, 27 (1995); ZEUS Collaboration, C.M. Ginsburg, in *8th International Workshop on Deep Inelastic Scattering*, DIS 2000, edited by J.A. Gracey and T. Greenshaw (World Scientific, Singapore, 2001), p. 537.
[35] V.M. Budnev *et al.*, Phys. Rep., Phys. Lett. **15C**, 182 (1975).
[36] OPAL Collaboration, G. Abbiendi *et al.*, Eur. Phys. J. C **14**, 199 (2000).
[37] L3 Collaboration, M. Acciarri *et al.*, Phys. Lett. B **505**, 47 (2001).
[38] OPAL Collaboration, G. Abbiendi *et al.*, Eur. Phys. J. C **18**, 15 (2000).
[39] OPAL Collaboration, K. Ackerstaff *et al.*, Phys. Lett. B **412**, 225 (1997).
[40] OPAL Collaboration, K. Ackerstaff *et al.*, Phys. Lett. B **411**, 387 (1997).
[41] L3 Collaboration, M. Acciarri *et al.*, Phys. Lett. B **436**, 403 (1998).
[42] L3 Collaboration, M. Acciarri *et al.*, Phys. Lett. B **447**, 147 (1999).
[43] ALEPH Collaboration, D. Barate *et al.*, Phys. Lett. B **458**, 152 (1999).
[44] L3 Collaboration, M. Acciarri *et al.*, Phys. Lett. B **453**, 83 (1999); **503**, 10 (2001); CERN-EP/2000-155 [Phys. Lett. (to be published)].
[45] OPAL Collaboration, G. Abbiendi *et al.*, Eur. Phys. J. C **16**, 579 (2000), and update in note OPAL PN 453.
[46] S. Frixione, M. Krämer, and E. Laenen, Nucl. Phys. **B571**, 169 (2000).
[47] M. Glück, E. Reya, and I. Schienbein, Phys. Rev. D **60**, 054019 (1999).
[48] ALEPH Collaboration, D. Buskulic *et al.*, Phys. Lett. B **355**, 595 (1995); and note ALEPH2000-070, ALEPH2000-031, in ICHEP2000, Osaka, Japan.
[49] DELPHI Collaboration, M. Chapkin, V. Obratztsov, and A. Sokolov, DELPHI2000-64, in ICHEP2000, Osaka, Japan.
[50] JADE Collaboration, W. Bartel *et al.*, Phys. Lett. B **184**, 288 (1987).
[51] TPC/2γ Collaboration, M. Alston-Garnjost *et al.*, Phys. Lett. B **252**, 499 (1990).
[52] TOPAZ Collaboration, R. Enomoto *et al.*, Phys. Lett. B **328**, 535 (1994).
[53] AMY-Collaboration, N. Takashimizu *et al.*, Phys. Lett. B **381**, 372 (1996).
[54] S.J. Brodsky, F. Hautmann, and D.E. Soper, Phys. Rev. D **56**, 6957 (1997).
[55] L3 Collaboration, M. Acciarri *et al.*, Phys. Lett. B **453**, 333 (1999).
[56] L3 Collaboration, contribution to XXX International Conference on High Energy Physics, Osaka, 2000, L3 Note 2568.
[57] OPAL Physics Note PN456, 2000.